

Directional dark matter detection sensitivity of a two-phase liquid argon detector

To cite this article: M. Cadeddu *et al* JCAP01(2019)014

View the [article online](#) for updates and enhancements.



IOP Astronomy ebooks

Part of your publishing universe and your first choice for astronomy, astrophysics, solar physics and planetary science ebooks.

iopscience.org/books/aas

Directional dark matter detection sensitivity of a two-phase liquid argon detector

M. Cadeddu,^{a,b,1} M. Lissia,^b P. Agnes,^{c,d} G. Batignani,^{e,f}
W.M. Bonivento,^b B. Bottino,^{g,h} M. Caravati,^{a,b} S. Catalanotti,^{i,l}
V. Cataudella,^{i,l} C. Cicalò,^b A. Cocco,^l G. Covone,^{i,l}
A. de Candia,^{i,l} G. De Filippis,^{i,l} G. De Rosa,^{i,l} S. Davini,^{h,m,n}
A. Devoto,^{a,b} C. Dionisi,^{o,p} D. Franco,^c C. Giganti,^q C. Galbiati,^{r,s}
S. Giagu,^{o,p} M. Gulino,^t M. Kuss,^f L. Lista,^l G. Longo,^{i,l}
A. Navrer-Agasson,^q M. Pallavicini,^{g,h} L. Pandola,^u E. Paoloni,^{e,f}
E. Picciau,^a M. Razeti,^b M. Rescigno,^p Q. Riffard,^c B. Rossi,^{l,r}
N. Rossi,ⁿ G. Testera,^h P. Trinchese,^{i,l} A. Tonazzo,^c S. Walker,^{i,l}
and G. Fiorillo^{i,l}

^aPhysics Department, Università degli Studi, Cagliari 09042, Italy

^bIstituto Nazionale di Fisica Nucleare, Sezione di Cagliari, Cagliari 09042, Italy

^cAPC, Université Paris Diderot, CNRS/IN2P3, CEA/Irfu,
Obs. de Paris, Sorbonne Paris Cité, Paris 75205, France

^dDepartment of Physics, University of Houston, Houston, TX 7704, U.S.A.

^ePhysics Department, Università degli Studi di Pisa, Pisa 56127, Italy

^fIstituto Nazionale Fisica Nucleare, Sezione di Pisa, Pisa 56127, Italy

^gPhysics Department, Università degli Studi di Genova, Genova 16146, Italy

^hIstituto Nazionale di Fisica Nucleare, Sezione di Genova, Genova 16146, Italy

ⁱPhysics Department, Università degli Studi Federico II and INFN,
Napoli 80126, Italy

^lIstituto Nazionale di Fisica Nucleare, Sezione di Napoli, Napoli 80126, Italy

^mGran Sasso Science Institute, L'Aquila AQ 67100, Italy

ⁿINFN Laboratori Nazionali del Gran Sasso, Assergi (AQ) 67010, Italy

^oPhysics Department, Sapienza Università di Roma, Roma 00185, Italy

^pIstituto Nazionale di Fisica Nucleare, Sezione di Roma 1, Roma 00185, Italy

^qLPNHE Paris, Université Pierre et Marie Curie,
Université Paris Diderot, CNRS/IN2P3,
Paris 75252, France

¹Corresponding author.

^rPhysics Department, Princeton University, Princeton, NJ 08544, U.S.A.

^sIstituto Nazionale di Fisica Nucleare, Sezione di Milano, Milano 20133, Italy

^tUniversità di Enna KORE, Enna 94100, Italy

^uIstituto Nazionale Fisica Nucleare, Laboratori Nazionali del Sud,
95123 Catania, Italy

E-mail: matteo.cadeddu@ca.infn.it

Received July 3, 2018

Revised November 27, 2018

Accepted December 17, 2018

Published January 4, 2019

Abstract. We examine the sensitivity of a large scale two-phase liquid argon detector to the directionality of the dark matter signal. This study was performed under the assumption that, above 50 keV of recoil energy, one can determine (with some resolution) the direction of the recoil nucleus without head-tail discrimination, as suggested by past studies that proposed to exploit the dependence of columnar recombination on the angle between the recoil nucleus direction and the electric field. In this paper we study the differential interaction recoil rate as a function of the recoil direction angle with respect to the zenith for a detector located at the Laboratori Nazionali del Gran Sasso and we determine its diurnal and seasonal modulation. Using a likelihood-ratio based approach we show that, with the angular information alone, 100 (250) events are enough to reject the isotropic hypothesis at three standard deviation level, for a perfect (400 mrad) angular resolution. For an exposure of 100 tonne years this would correspond to a spin independent WIMP-nucleon cross section of about 10^{-46} cm² at 200 GeV WIMP mass. The results presented in this paper provide strong motivation for the experimental determination of directional recoil effects in two-phase liquid argon detectors.

Keywords: dark matter detectors, dark matter experiments

ArXiv ePrint: [1704.03741](https://arxiv.org/abs/1704.03741)

Contents

1	Introduction	1
2	Recoil rates	3
2.1	Cross section and differential rates	3
2.2	Recoil rate in Galactic angular coordinates	6
3	Recoil directional signals at LNGS	7
3.1	Differential rates as functions of the polar angle	8
3.2	Vertical and horizontal event categories	8
4	Seasonal effects	10
5	Statistical analysis for a directional signal	12
6	Conclusions	14

1 Introduction

Dark Matter (DM) is the most compelling indirect evidence for physics beyond the Standard Model. It constitutes about 80% of the mass of the Universe [1] and has a fundamental role in the comprehension of the evolution of the Universe since the Big Bang. Understanding the nature of DM is therefore one of the most intriguing puzzles in physics. In the last decades many measurements have been gathered that could be explained by assuming a large amount of DM in cosmic structures at different mass scales. Starting from rotation curves of spiral galaxies [2], the most persuasive evidences come from the observations of anisotropies of the Cosmic Microwave Background [1], gravitational lensing on galaxy clusters [3] and galaxy scales [4], and the Big-Bang nucleosynthesis [5]. A plausible model for DM is that it consists of non-relativistic Weakly-Interacting Massive Particles (WIMPs). In our Galaxy, the density distribution of this DM halo, which extends far beyond the visible disk, are inferred from the rotation curves of the visible matter [6, 7]. The velocity distribution is less understood but it can be inferred using different approaches [8–10].

Direct detection DM experiments look for possible WIMP interactions with target nuclei aiming to detect an excess of WIMP-induced nuclear recoils above the estimated background [11]. Establishing this excess is a serious experimental challenge, given the expected electron and neutron backgrounds that mimic nuclear recoils from WIMPs and the low expected rate. It is necessary to remove radioactive backgrounds to a technologically-challenging low level and to rely on the detector capability to discriminate the remaining backgrounds. A non-directional detector could enhance the signal over background ratio using the expected annual modulation of the DM signal due to the Earth motion around the Sun [12, 13]. For instance the DAMA collaboration [14, 15] reported an observation of such a modulation. However, this seasonal modulation is expected to be smaller than 10% and background sources exist that have similar seasonal modulations [16].

A large mass detector with sensitivity to the direction of the recoiling nuclei would constitute a considerable breakthrough in the search for DM, as we shall argue in this work. A directional detector would allow one to prove that the detected new particle is indeed a dark matter candidate.

For the sake of concreteness a detector located at the latitude¹ of the INFN Laboratori Nazionali del Gran Sasso (LNGS), Italy, where the DarkSide-20k experiment [17] will be located, is considered.

We show that the expected event rate varies by a large factor (4–8) when considering nuclear recoil directions going from the zenith to the horizon and, at fixed angular direction, it varies by about the same factor with sidereal-day period. The angular resolution of the detector will imply important consequences on the experimental sensitivity to such a rate variation. The event-rate variations as a function of the sidereal time and as a function of the polar angle are very robust and are largely independent on details of the WIMP interaction and of the WIMP velocity distribution: they are direct consequences of the solar system motion through the Galaxy, the Earth revolution around the Sun and its rotation. Isotropic backgrounds (e.g. diffuse supernovae and atmospheric neutrinos), backgrounds from sources within the solar system (e.g. solar neutrinos), or backgrounds with the periodicity of solar day (e.g. backgrounds that depend on the temperature or the atmospheric density) can be considerably reduced using the angular and time information provided by a directional detector.

Several prototypes of directional detectors exist [18, 19], generally based on the attempt to perform an imaging of the nuclear recoil trajectory. These detectors aim at achieving high spatial resolutions and are usually limited in mass, thus being capable to collect limited exposures. On the other hand, non-directional DM detectors have already reached exposures greater than 10^5 kg-day, [20] excluding spin independent WIMP-nucleon cross section lower than about 1.7×10^{-46} cm² for a 200 GeV WIMP mass.

As argued in [21], a promising technique for a very large-mass detector with directional DM capability would be to exploit the phenomenon called *Columnar Recombination* (CR) in a noble liquid Time Projection Chamber (TPC). An argon-based detector sensitive to the effect of CR, would combine directional sensitivity with the ability to collect exposures of several hundreds of tonnes year [17].

In noble liquid TPCs the recoiling nucleus produces both scintillation and ionization. CR models [22, 23] predict that the amount of signal due to ionization that can be collected in the presence of an electric field $\vec{\mathcal{E}}$ should depend on the angle θ_r between $\vec{\mathcal{E}}$ and the track (the average direction of the straggling nucleus). The ionization signal is expected to be maximal when $\theta_r = 90^\circ$, since electrons drift in a direction perpendicular to the region around the recoil track where ions are present, minimizing recombination. On the contrary, it should be minimal when $\theta_r = 0^\circ$, since electrons drift along the region where ions are present, with high probability of recombination. The ionization signal from the collected electrons would be a function of the component of the electric field perpendicular to the track, $\mathcal{E}_\perp = \mathcal{E} \sin \theta_r$, and, therefore would carry, together with the scintillation signal, information on the average direction of the recoiling nucleus. CR in a Liquid Argon (LAr) TPC would thus provide signatures for the orientation of the ionizing tracks relative to the direction of electric field. Evidence for this effect has been collected for α particles and protons [24, 25] with energies of 5.14 MeV and between 50–250 MeV, respectively. The SCENE experiment [26, 27], a small two-phase LAr TPC designed for calibration of nuclear-recoil responses, gave a hint for the same directional signature in the scintillation response of nuclear recoils of about 57 keV, approximately the energy at which, following the argument in [21], one might expect the ion range to be sufficient to form a track with a definite direction.

¹The LNGS coordinates are 42° 28' N 13° 33' E.

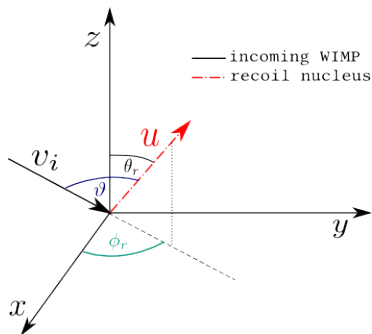


Figure 1. Schematic view of a WIMP-nucleus scattering in a reference frame such that x , y and z are laboratory-fixed coordinates. The incoming WIMP with velocity \mathbf{v}_i hits the nucleus that recoils in the direction of the momentum $\mathbf{q} = m_N \mathbf{u}$ whose azimuthal and polar angles are ϕ_r and θ_r . The angle between u and \mathbf{v}_i is ϑ .

General aspects of DM directional detection have been discussed in a number of papers [18, 28–30]. In the following, an active mass of 100 tonne (which in terms of number of WIMP events is equivalent to a 20 tonne active mass detector running for 5 years) is considered with a detector at LNGS as in the DarkSide-20k experiment [17]. Namely, DarkSide-20k will be able to collect such exposure keeping the number of instrumental background interactions to less than 0.1 events. At the location of the laboratory, the angle between the expected average WIMP direction with the vertical electric field in the LAr TPC spans the entire range between 0° and 90° during the day. Preliminary results have been presented in conference proceedings [31–33], but the statistical analysis, seasonal modulation and the application to larger detectors are shown for the first time in this paper.

The paper is outlined as follows. Section 2 reviews the theoretical framework, introducing the formulae for the recoil cross section and rates as a function of the relevant angular variable, velocity distribution and coordinate systems. Section 3 presents the recoil angular distributions, while section 4 discusses the annual modulation of the signals. Section 5 presents a simplified statistical analysis method to study the DM directionality. We draw our conclusions in section 6.

2 Recoil rates

2.1 Cross section and differential rates

In a given reference frame, let's assume \mathbf{v}_i is the velocity of the incoming WIMP of mass m_χ , \mathbf{u} is the velocity of the recoiling nucleus of mass m_N , $\mathbf{q} = m_N \mathbf{u}$ is the nucleus momentum and $E_r = q^2/(2m_N)$ is the corresponding energy. The azimuthal and polar angles of the recoiling nucleus are ϕ_r and θ_r , while ϑ is the angle between the incoming WIMP direction and the recoiling nucleus, as shown in figure 1. In general, recoil rates are convolutions of the scattering cross section and the incoming velocity distribution. A point-like cross section in the center of mass is constant and can be parametrized by the total WIMP-nucleus cross section $\sigma_{\chi-N}$. For a spin-independent interaction with equal couplings for neutrons and protons, $\sigma_{\chi-N}$ can be expressed in terms of WIMP-nucleon cross section σ_n as $\sigma_{\chi-N}/\mu_N^2 = A^2 \sigma_n/\mu_p^2$, where A is the atomic mass and μ_N and μ_p are the WIMP-nucleus and the WIMP-nucleon reduced masses, respectively. The finite size of the nucleus is taken

into account by introducing the Helm nuclear form factor [34]:

$$F(q) = \frac{3 [\sin(qr_N) - qr_N \cos(qr_N)]}{(qr_N)^3} e^{-(qs)^2/2}, \quad (2.1)$$

where $s = 0.9$ fm is the surface thickness and $r_N = 3.9$ fm is the argon nucleus effective radius.

In the laboratory frame, where the target nucleus is at rest, the double-differential cross section depends on the cosine of the angle between the incoming WIMP and the recoiling nucleus $\hat{\mathbf{v}}_i \cdot \hat{\mathbf{q}} = \cos \vartheta$ as

$$\begin{aligned} \frac{d^2\sigma(q, \hat{\mathbf{v}}_i \cdot \hat{\mathbf{q}})}{dq^2 d\Omega} &= \frac{d^2\sigma(q, \cos \vartheta)}{2m_N dE_r 2\pi d\cos \vartheta} \\ &= \frac{\sigma_{\chi-N}}{8\pi\mu_N^2 v_i} F^2(q) \delta\left(\mathbf{v}_i \cdot \hat{\mathbf{q}} - \frac{q}{2\mu_N}\right). \end{aligned} \quad (2.2)$$

Given a velocity distribution for the incoming WIMP $f(\mathbf{v}_i)$, normalized so that $\int f(\mathbf{v}) d\mathbf{v} = 1$, and a WIMP mass density ρ , the double-differential recoil rate per unit mass, i.e. the rate per target nucleus divided by the nucleus mass m_N , as a function of the nuclear recoil energy, E_r , and of the recoil direction $\hat{\mathbf{q}}$ is

$$\begin{aligned} \frac{d^2R(E_r, \hat{\mathbf{q}})}{dE_r d\Omega_r} &= \frac{2\rho}{m_\chi} \int v \frac{d^2\sigma(q, \hat{\mathbf{v}} \cdot \hat{\mathbf{q}})}{dq^2 d\Omega} f(\mathbf{v}) d\mathbf{v} \\ &= \frac{\rho \sigma_{\chi-N} F^2(q)}{m_\chi 4\pi \mu_N^2} \int \delta\left(\mathbf{v} \cdot \hat{\mathbf{q}} - \frac{q}{2\mu_N}\right) f(\mathbf{v}) d\mathbf{v} \\ &= \frac{\rho}{m_\chi} \frac{\sigma_{\chi-N} F^2(q)}{4\pi \mu_N^2} \hat{f}(v_{\min}, \hat{\mathbf{q}}), \end{aligned} \quad (2.3)$$

where $v_{\min} = q/(2\mu_N) = \sqrt{2m_N E_r}/(2\mu_N)$ is the minimal WIMP velocity that can give momentum q or energy E_r to the recoiling nucleus and $\hat{f}(v_{\min}, \hat{\mathbf{q}})$ is the 3-dimensional Radon transform [35] of the velocity distribution $f(\mathbf{v})$.

In this paper we assume the Standard Halo Model (SHM), i.e. an isotropic Maxwell-Boltzmann WIMP velocity distribution of width σ_v in a reference frame at rest with respect to the Galactic center.² In a reference frame with velocity \mathbf{V} relative to the Galactic center, the velocity distribution is

$$f(\mathbf{v}) = \frac{1}{\sqrt{(2\pi\sigma_v^2)^3}} \exp\left[-\frac{1}{2} \left(\frac{\mathbf{v} + \mathbf{V}}{\sigma_v}\right)^2\right] \quad (2.4)$$

and the corresponding Radon transform is

$$\hat{f}(v_{\min}, \hat{\mathbf{q}}) = \frac{1}{\sqrt{2\pi\sigma_v^2}} \exp\left[-\frac{1}{2} \left(\frac{v_{\min} + \hat{\mathbf{q}} \cdot \mathbf{V}}{\sigma_v}\right)^2\right]. \quad (2.5)$$

Therefore, if recoils are measured in a frame at rest with respect to the center of the Galaxy, $\mathbf{V} = 0$ and the rate is isotropic. Similarly, when measured in a frame at rest with respect to the Sun, \mathbf{V} is the Sun velocity relative to the galactic center \mathbf{V}_{SG} , which points towards the galactic coordinates [37] ($\ell_c = 90^\circ$, $b_c = 0^\circ$), roughly the direction of the Cygnus constellation, and has magnitude $V_{\text{SG}} \approx v_0 = 220$ km/s, where v_0 is the Galactic orbital speed at the Sun position. For an Earthbound laboratory the velocity \mathbf{V} can be decomposed as

²The usage of a truncated velocity distribution at the escape velocity of 544 km/s (see ref. [36] for details) has a negligible impact on the event rate and on the rate distributions.

$\mathbf{V} = \mathbf{V}_{\text{SG}} + \mathbf{V}_{\text{ES}}$, where \mathbf{V}_{ES} is the Earth velocity relative to the Sun, which has magnitude $V_{\text{ES}} \approx 30$ km/s, about ten times smaller than v_0 . The laboratory speed relative to the Earth center has been neglected, since it is almost two orders of magnitude smaller than \mathbf{V}_{ES} and the contribution to the rate is negligible. Clearly, its direction is accounted for being the crucial ingredient for the directional detection.

If a detector collects events of energy $E_{\text{th}} < E_r < E_{\text{max}}$, the direction-dependent recoil rate per unit mass, obtained by substituting the Radon transform from eq. (2.5) in eq. (2.3) and integrating over the energy range, becomes

$$\frac{dR(E_{\text{th}}, E_{\text{max}}, \hat{\mathbf{q}})}{d\Omega_r} = \int_{E_{\text{th}}}^{E_{\text{max}}} dE_r \frac{d^2 R(E_r, \hat{\mathbf{q}})}{dE_r d\Omega_r}. \quad (2.6)$$

The study presented in this paper focuses on the use of polar detectors i.e. detectors that give only information on the angle θ_r between the recoil track and a fixed axis. If the fixed axis is the vertical direction, which corresponds to the z-axis as in figure 1, the relevant recoil rate is

$$\frac{dR(E_{\text{th}}, E_{\text{max}}, \cos \theta_r)}{d \cos \theta_r} = \int_0^{2\pi} d\phi_r \int_{E_{\text{th}}}^{E_{\text{max}}} dE_r \frac{d^2 R(E_r, \hat{\mathbf{q}})}{dE_r d\Omega_r}, \quad (2.7)$$

which, after integrating out ϕ_r , depends on $\cos \theta_r$. In addition, if a detector cannot distinguish signals from recoil tracks differing by 180° , events that differ by 180° are summed together. The relevant rate is the so-called “folded” angular recoil rate [38]:

$$\frac{dR_F(|\cos \theta_r|)}{d|\cos \theta|} \equiv \frac{dR}{d \cos \theta_r}(\cos \theta_r) + \frac{dR}{d \cos \theta_r}(-\cos \theta_r), \quad (2.8)$$

which depends only on $|\cos \theta_r|$. Dependences of the recoil rates on other variables are not shown.

Unless explicitly stated, this work shows results for a LAr detector using the reference values $m_\chi = 200$ GeV, $m_N = 0.923 A$, where A is the argon atomic mass, $\rho = 0.3$ GeV cm $^{-3}$, and $\sigma_v = v_0/\sqrt{2}$. Rates are given for a reference cross section $\sigma_n = 10^{-46}$ cm 2 , which is of the order of the last limits set by the LUX, Xenon1T and PANDAX-II collaborations [39–41], for recoil energies from $E_{\text{th}} = 50$ keV to $E_{\text{max}} = 200$ keV, and for an active mass of 100 tonne.³ Note that the anisotropy of all rates in eqs. (2.6), (2.7), and (2.8) depends only on the velocity \mathbf{V} . In a given frame, which fixes \mathbf{V} , one can choose different angular coordinate systems. If the angular coordinate system is time dependent, *e.g.* a coordinate system fixed to the rotating Earth, the direction of \mathbf{V} in that system becomes time dependent. In a frame at rest with respect to the Earth and using Galactic coordinates, \mathbf{V}_{SG} is constant and only \mathbf{V}_{ES} rotates with the annual periodicity of the Earth revolution. Since \mathbf{V}_{ES} is an order of magnitude smaller than \mathbf{V}_{SG} , the WIMP apparent direction $-\mathbf{V} = -(\mathbf{V}_{\text{SG}} + \mathbf{V}_{\text{ES}})$ rotates with annual periodicity around the fixed \mathbf{V}_{SG} direction with an opening angle of about one tenth of radian. In this frame the peaked angular distribution is the main signature of the signal and allows for background reduction. In the laboratory coordinate system, the coordinates and, therefore, the apparent direction of \mathbf{V} makes an additional rotation with the periodicity of a sidereal day and an amplitude that depends on the latitude. This specific periodicity is also a characteristic signature and provides more background suppression.

³This choice for the threshold energy is motivated by hints from the SCENE experiment [27] for directional dependence in the scintillation signal at energy of 57.3 keV.

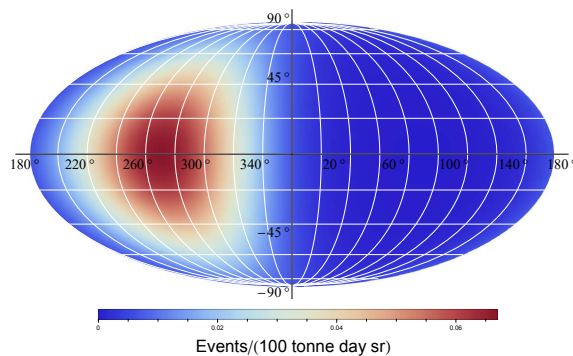


Figure 2. Recoil rate in argon, eq. (2.6), on a Mollweide equal area projection map of the celestial sphere in galactic coordinates. The horizontal axis is the galactic longitude $0^\circ < \ell < 360^\circ$ and the vertical axis is galactic latitude $-90^\circ < b < 90^\circ$. The WIMP mass is 200 GeV, the WIMP-nucleon cross section 10^{-46}cm^2 and the energy interval ($50 \text{ keV} \leq E_r \leq 200 \text{ keV}$). The color scale is units of events/(100 tonne \cdot day \cdot sr).

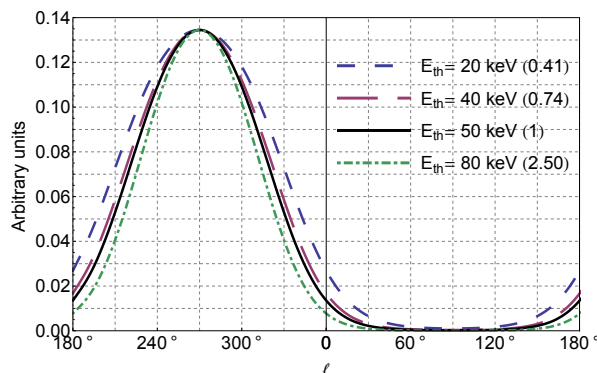


Figure 3. Recoil rate in arbitrary units for argon as a function of the galactic longitude ℓ in degrees. The WIMP mass is assumed to be 200 GeV and the recoil energy is integrated between E_{th} and 200 keV, where $E_{\text{th}} = 20, 40, 50$ and 80 keV. With respect to the curve for $E_{\text{th}} = 50 \text{ keV}$ the other curves have been rescaled to have the same maximum. As shown in the legend the rescaling factors are: 0.41, 0.74, 2.50, respectively.

2.2 Recoil rate in Galactic angular coordinates

Figures 2 and 3 show results in a reference frame at rest with respect to the Sun in Galactic coordinates to demonstrate the potentialities of a directional detector independently of the location, as it has been extensively done in the past, and to discuss the influence of the threshold energy E_{th} . All other results will be given for a detector located at the latitude of LNGS in the local coordinate system with the polar axis pointing in the vertical direction. Indeed, the potentialities of a directional detector and, more specifically, the signature in the angular recoil rate of the detector motion through the WIMP halo are best illustrated in Galactic coordinates in a frame at rest with the Sun. In this coordinate system, \hat{x} points from the Sun towards the Galactic center, \hat{y} in the direction of the Solar motion and \hat{z} towards the Galactic north pole; therefore, $\mathbf{V} = v_0 \hat{y}$. In figure 2 we show the angular recoil rate of eq. (2.6) for argon on a Mollweide equal area projection map. The horizontal axis is the galactic longitude $0^\circ < \ell < 360^\circ$ (the counterclockwise angle from the \hat{x} axis) and the

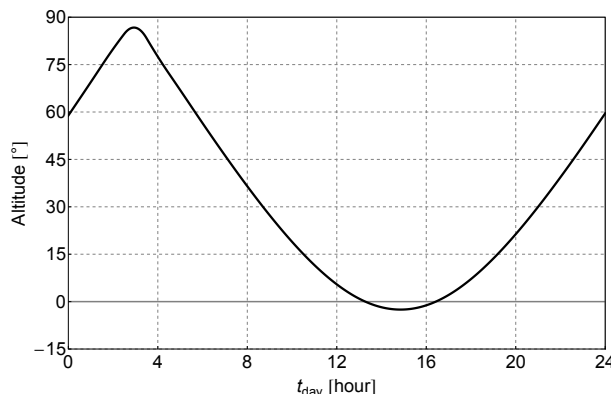


Figure 4. Altitude (angle above the horizon) of the Cygnus constellation as seen at LNGS as a function of the local clock time. The horizontal line at 0° corresponds to the horizon.

vertical axis is the galactic latitude $-90^\circ < b < 90^\circ$ ($90^\circ - b$ is the angle from the \hat{z} axis). To obtain the total number of events that are expected for an exposure of 100 tonne year, one has to integrate over the solid angle and multiply by 365 days. This results in a number of WIMPs above 50 keV of about 74. With the same assumption on the WIMP mass and the WIMP-nucleon cross section, the total number of WIMP events expected from DarkSide-20k for 5 years of data taking including the proper nuclear recoil acceptance as in ref. [17], is about 100 since it includes events below 50 keV, which we conservatively do not include when considering a directional detector.

The recoil rate is clearly anisotropic [29] and points at coordinates ($l = 270^\circ, b = 0^\circ$) opposite to the direction of the Sun motion throughout the Galaxy. Since the expected signal in the SHM is rotationally symmetric around the Sun direction, the width of the forward peak is better shown on one dimensional plot as a function of the galactic longitude l , obtained integrating over the galactic latitude b (figure 3). The units on the y -axis are events/(100 tonne day $180/\pi$), such that after integration one obtain about 0.2 events/(100 tonne day). In figure 3 the effect of different energy thresholds is considered. Indeed, it shows that the width of the peak is slightly reduced for higher recoil energies, thus increasing the correlation between the recoil direction and the apparent WIMP arrival direction, even if the width of the peak is dominated by the WIMP transverse velocity distribution. Indeed, in a liquid the straggling of the recoiling nucleus will broaden further the peak. A higher threshold, in addition, lowers the total rate as it can be quantitatively seen from the normalization factors.

3 Recoil directional signals at LNGS

In this section we consider WIMP scattering in a reference frame at rest relative to a detector situated at LNGS with the \hat{z} axis (anti-parallel to the drift electric field direction) along the local vertical. In this frame we call the angle between the recoiling nucleus and the vertical axis θ_r . In particular we study the expected rates, eqs. (2.6) and (2.8), as function of $\cos \theta_r$ and of the time of the day. The effect of finite angular resolution is also considered.

Figure 4 shows the Cygnus constellation altitude at the LNGS location as a function of the local clock time from the midnight of the Summer Solstice (SS), providing a clear picture of the daily dependence of the expected recoil *average* direction. As already discussed the

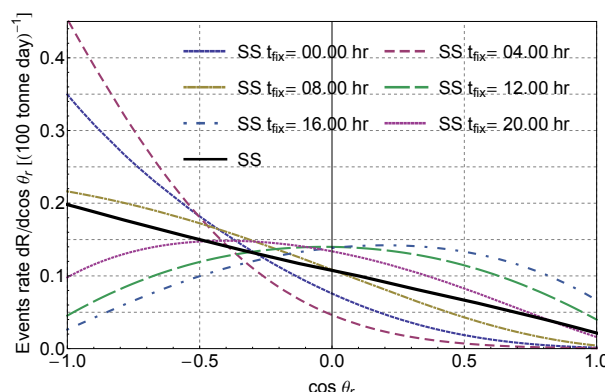


Figure 5. Differential recoil rate as a function of the cosine of the polar angle θ_r (the angle between the recoil direction and the z axis) at the latitude of LNGS for the SS day (solid black line). The six dashed curves show the differential recoil rate obtained freezing the position of the Cygnus in the sky at a given time (four-hour apart from each other) of the SS day for the whole day.

correlation between the Cygnus direction and the WIMP wind changes by at most a tenth of radian during the year because of the Earth revolution around the Sun. As the cross section in eq. (2.2) peaks in the forward direction, when Cygnus is close to the zenith on average nuclei recoil mainly towards the nadir, and when Cygnus is close to horizon on average nuclei recoil mainly in the horizontal plane. The most important qualitative feature in figure 4 is that Cygnus spans the whole range of polar directions from zenith to horizon during the day at the LNGS latitude, thus allowing a strong correlation between time and polar angle of the recoils. Since the Cygnus polar angle period is the sidereal day, this correlation is lost during the year if local solar time is used.

3.1 Differential rates as functions of the polar angle

Figure 5 shows the differential recoil rate, eq. (2.7), as a function of $\cos \theta_r$ for the SS day (solid black line). This rate is more than twice as high for negative values of $\cos \theta_r$ than for positive values, since Cygnus is most of the time above the horizon. Freezing the position of the Cygnus in the sky at a given time of the SS day for the whole day, one obtains the different dashed lines in figure 5. One clearly sees that there is a strong dependence on the time of the day. Indeed, the asymmetry in $\cos \theta_r$ (the angle between the recoil direction and the z axis) is larger when Cygnus is high in the sky, e.g., at hour 4, while it is smaller when it is close to the horizon, e.g., at hour 16.

Figure 6 shows the “folded” differential recoil rate introduced in eq. (2.8), the relevant rate for a polar detector. The angular and time dependences of the rate remain quite strong even without the information on which side of the track the head is. When Cygnus is close to the zenith (horizon) the rate is peaked at $|\cos \theta_r| \sim 1$ ($|\cos \theta_r| \sim 0$).

3.2 Vertical and horizontal event categories

A simple and robust analysis of the time and angular dependency of the event rate of WIMP collision is achieved by separating the candidate event sample into two categories that require only a minimal amount of angular information. Events can be categorized as horizontal events (HOR), defined by $|\cos \theta_r| < 0.5$ or $60^\circ < \theta_r < 120^\circ$, and vertical events (VER), defined by $|\cos \theta_r| > 0.5$ (see figure 7).

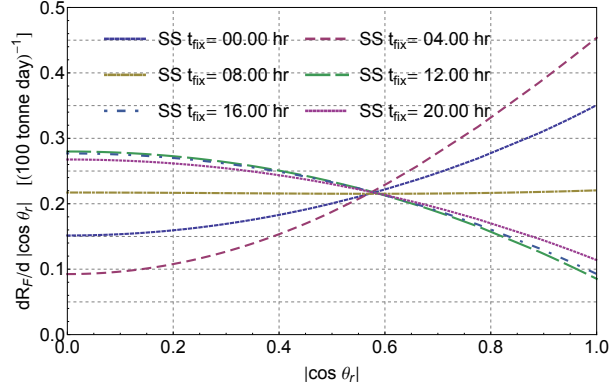


Figure 6. Same as figure 5 for the “folded” rate in eq. (2.8).

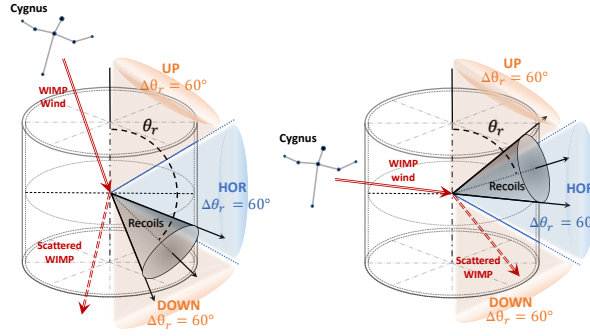


Figure 7. Schematic view of the two categories in which events are divided, namely horizontal (HOR) and vertical (VER=UP+DOWN) events for two different Cygnus altitudes in the sky.

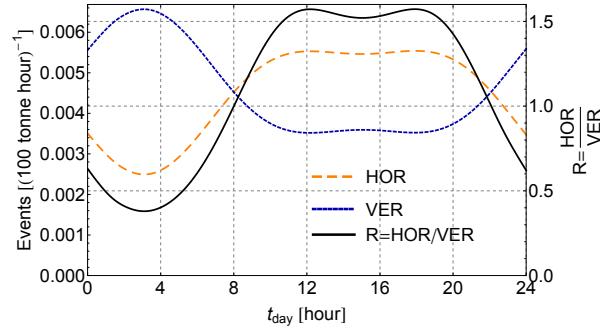


Figure 8. Horizontal (HOR), corresponding to $|\cos \theta_r| < 0.5$ or $60^\circ < \theta_r < 120^\circ$ (long dashes) and vertical (VER), corresponding to $|\cos \theta_r| > 0.5$ (short dashes) event rates as a function of time in event per 100 tonne per hour (left scale). The solid line shows the ratio $R = \text{HOR}/\text{VER}$ (right scale). Curves are drawn for the summer solstice day.

Figure 8 shows horizontal and vertical WIMP event rates as function of the time of the day. At the latitude of LNGS, the time signature of an anisotropic WIMP wind is evident in spite of the very crude angular classification. In the same figure we also show the ratio $R = \text{HOR}/\text{VER}$ of horizontal to vertical events. For the given choice of parameters, R changes during the day by a factor of about 4.

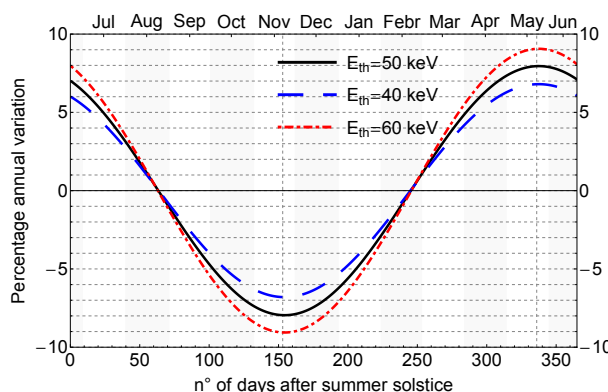


Figure 9. Percentage annual variation of the argon detector event rate as a function of the number of days from the summer solstice for three different recoil energy thresholds. The solid line corresponds to $E_{\text{th}} = 50$ keV, the dotted line corresponds to $E_{\text{th}} = 40$ keV, and the dashed line corresponds to $E_{\text{th}} = 60$ keV. The corresponding average daily rates are 0.21, 0.27, and 0.15 events per day for a 100 tonne active mass.

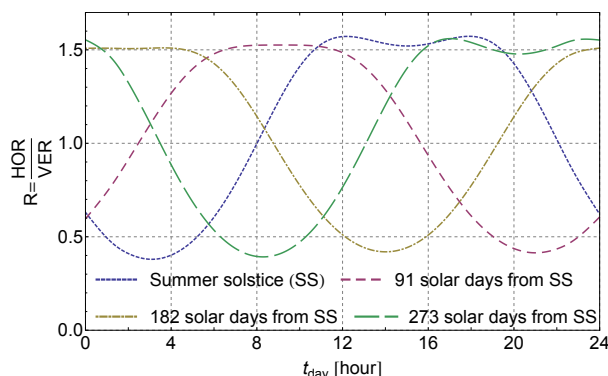


Figure 10. Ratio R of expected number of events along the horizontal and the vertical direction in an argon detector located at LNGS as function of the time of the day at four different days of the year. R is defined in figure 8 and in the text referring to it.

4 Seasonal effects

As already discussed in section 2.1, the Earth velocity within the Galaxy and, therefore, the velocity relative to the average WIMP velocity $\mathbf{V} = \mathbf{V}_{\text{SG}} + \mathbf{V}_{\text{ES}}$ changes during the year due to the annual rotation of orbital velocity \mathbf{V}_{ES} . Since $|\mathbf{V}_{\text{SG}}| \approx 220$ km/s and $|\mathbf{V}_{\text{ES}}| \approx 30$ km/s with an angle of about 60° between \mathbf{V}_{SG} and the ecliptic, the module $|\mathbf{V}|$ changes by about $\pm 15/220 \approx \pm 7\%$ during the year causing a similar change of the WIMP flux, while the annual change of direction is about a tenth of radian. This annual change of the average WIMP speed produces a corresponding change of the total daily rate, which reaches its maximum around the end of May and its minimum around the end of November, as clearly visible in figure 9 for three threshold energies: $E_{\text{th}} = 40, 50$, and 60 keV. As expected [42, 43] the larger the energy threshold the larger the percentage annual modulation.

Figure 10 shows the daily variation of the ratio R at four times of the year; the signal time structure changes during the year as function of the local time. Cygnus, i.e. the WIMP

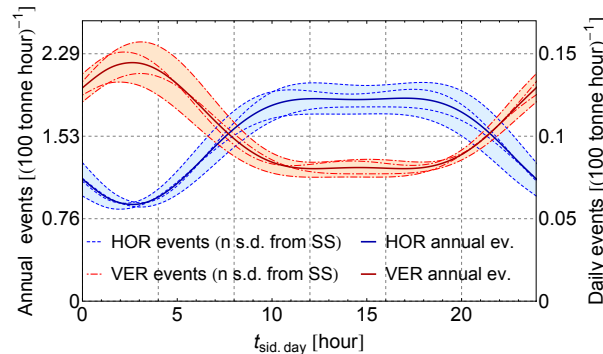


Figure 11. Solid red and blue lines (left y-scale): annual sum of $\text{HOR} \equiv |\cos \theta_r| < 0.5$ and vertical ($\text{VER} \equiv |\cos \theta_r| > 0.5$) events expected at each hour of a sidereal day, respectively. Dashed red and blue lines (right y-scale): events at each hour of a given sidereal day, namely the day of the SS, and 91, 182, 273 days after it.

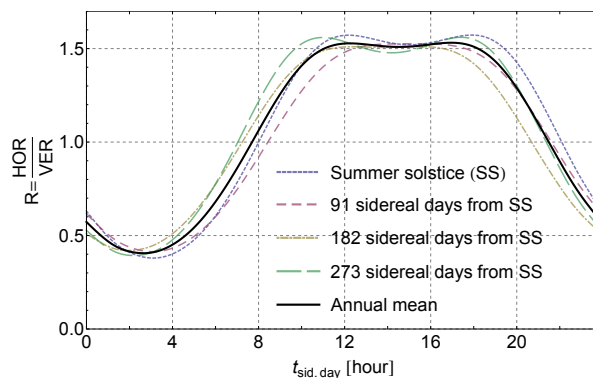


Figure 12. Same as figure 11 for the ratio $R = \text{HOR}/\text{VER}$.

direction, returns exactly in the same position in the sky after a sidereal day, which is about four minutes shorter than the solar day. This annual drift of the angular signal as a function of the solar time can be used to characterize the WIMP signal with respect to other effects that also produce daily variations but with solar-day periodicity [44].

If the sidereal time is used to time-stamp events, the annual drift is eliminated and it is possible to compare and average events rates taken at different days. Figure 11 shows the HOR and VER daily event rates taken at four times of the year and the annual rates of HOR and VER events computed by summing the contributions at each sidereal day. Figure 12 shows for R the same information as figure 11 for HOR and VER. Note that part of the seasonal variation of HOR and VER cancels out in their ratio R .

The much larger time variation of the directional signal relative to the seasonal variation of the non-directional signal is evident by comparing figure 9 to figure 12, or also in figure 10 or figure 11. However one should use the combination of seasonal and directional modulations to better characterize the nature of the signal.

5 Statistical analysis for a directional signal

A path through the discovery process of DM searches may proceed initially through the observation of a number of candidates that significantly exceed the small expected background level. However, after rejecting the background-only hypothesis, the study of angular properties of the observed nuclear recoils can corroborate the belief that the observed signal can be attributed to DM interactions. In section 3 we have discussed semi-quantitatively the power of angular discrimination by using a crude classification in horizontal and vertical events. Here we want to quantitatively discuss the number of events necessary to discriminate the hypothesis of a DM signal with preferential incoming direction from the Cygnus constellation against the alternative hypothesis of an isotropic signal.

The negative logarithm of the likelihood ratio is taken as test statistic t to discriminate between the hypotheses of a directional signal from the Cygnus constellation (Cyg) against an isotropic signal (iso) (\mathbf{V} as in section 2.1 or $\mathbf{V} = 0$, respectively). Such test statistic can also be extended in order to take into account the effect of systematic uncertainties for realistic applications [45]. The test statistic is defined as

$$t(\vec{x}^{(1)}, \dots, \vec{x}^{(N)}) = -\ln \frac{\mathcal{L}_{\text{Cyg}}(\vec{x}^{(i)})}{\mathcal{L}_{\text{iso}}(\vec{x}^{(i)})}, \quad (5.1)$$

where $\mathcal{L}_{\text{Cyg,iso}}(\vec{x}^{(i)})$ are the likelihood functions corresponding to the two hypotheses. Given a sample of N independent WIMP events, the two likelihood functions are given by the products of the probability density function (PDF) values $f_{\text{Cyg,iso}}(\vec{x}^{(i)})$ corresponding to each WIMP interaction candidate:

$$\mathcal{L}_{\text{Cyg,iso}}(\vec{x}^{(1)}, \dots, \vec{x}^{(N)}) = \prod_{i=1}^N f_{\text{Cyg,iso}}(\vec{x}^{(i)}), \quad (5.2)$$

where the vector $\vec{x}^{(i)}$ contains the variables used to characterize the event (i). In the present work we use the two variables θ_{rec} , the recoil polar angle in the laboratory, and θ_{Cyg} , the polar angle of the Cygnus constellation at time of the event in the laboratory: $\vec{x}^{(i)} \equiv (\theta_{\text{rec}}^{(i)}, \theta_{\text{Cyg}}^{(i)})$. Additional variables such as the recoil energy or the time of the year could provide additional information and, in principle, better discrimination between the two hypotheses, our conclusions are conservative in this respect. The same method can be used to study alternative models for WIMP distribution or backgrounds.

The PDFs $f_{\text{Cyg,iso}}(\vec{x}^{(i)})$ have been sampled generating 10^{10} simulated interaction recoils for each hypothesis and binning the allowed kinematic range of each variable $\theta_{\text{rec}}^{(i)}$ and $\theta_{\text{Cyg}}^{(i)}$ with 100 bins. In the simulation the energy has been smeared by 10 keV in order to account for the energy resolution and an energy threshold of 50 keV has been used. In addition we compared the case of perfect resolution of the recoil angle in the laboratory frame to a resolution smeared by a Gaussian distribution with a 400 mrad width.

Given an assumed number N of WIMP interaction candidate events, 10^7 pseudo-samples of N events each were generated for each of the four cases, namely events from Cygnus direction or isotropic and with the two angular resolutions. The test statistic, t , of eq. (5.1) has been evaluated for each pseudo-sample and stored into histograms with a fine binning. Figure 13 shows the distribution of the test statistic t defined in eq. (5.1) for the case of ideal (left panel) and 400 mrad resolution (right panel) with $N = 50$. The directional (isotropic) distribution is peaked at negative (positive) values. The expected p -value is computed from

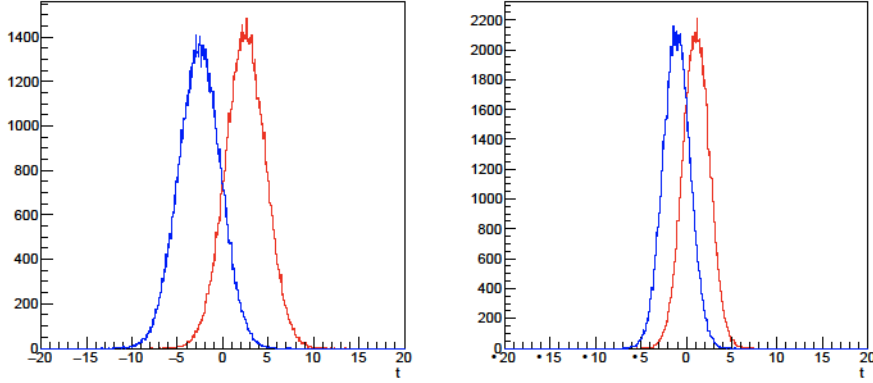


Figure 13. Distribution of the likelihood-ratio test statistic t for ideal resolution (left) and for a resolution of 400 mrad (right) for $N = 50$ observed DM candidates. The blue (red) curves that peak at negative (positive) values of t correspond to the hypothesis of incoming particles from the Cygnus direction (of isotropic signal).

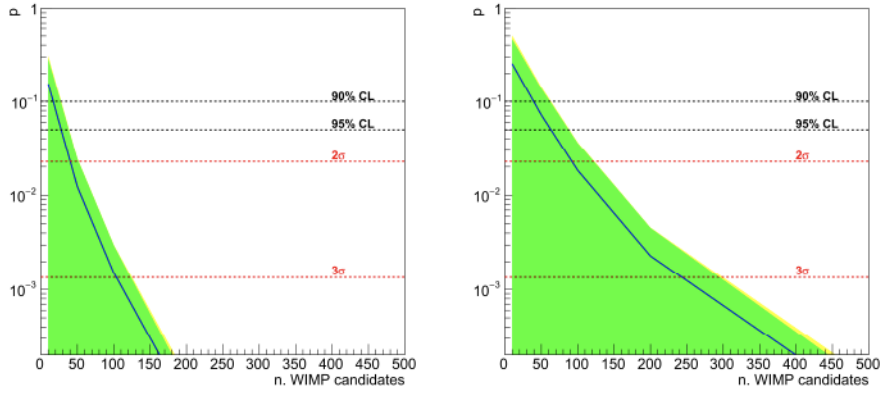


Figure 14. Expected p -value (blue line) of the null hypothesis (isotropic signal) as a function of the observed number of DM interaction candidate events for ideal resolution (left) and for a resolution of 400 mrad (right). The green and yellow bands show the excursion range at one and two standard deviations. The horizontal lines show from top to bottom the 90% and 95% CL exclusion and the 2σ and 3σ significance levels.

the distribution of the test statistic t_{iso} corresponding to the null (isotropic) hypothesis by considering the percentage of pseudo-sample with t below $t_{\text{Cyg},0}$, where $t_{\text{Cyg},0}$ is the median of the distribution of the test statistic t_{Cyg} corresponding to Cygnus direction hypothesis. The corresponding one- or two-standard-deviation excursions are calculated by considering instead of $t_{\text{Cyg},0}$ the boundaries of the one- or two-standard-deviation interval for the test statistic t_{Cyg} .

The expected p -values as a function of the observed number of DM interaction candidate events are shown in figure 14 for ideal angular resolution (left) and for a 400 mrad resolution (right). In the case of an ideal resolution, a 3σ evidence of a directional signal is expected to be achieved with about 100 candidate events. For an angular resolution of 400 mrad, a 3σ evidence can be achieved with about 250 events.

6 Conclusions

We examined the sensitivity of a large scale dark matter liquid argon experiment to the directionality of the dark matter signal, under the assumption that it is possible, above a certain threshold, to measure the direction of the recoiling nucleus. This may indeed be possible with two-phase liquid argon detectors, if the suggested dependence of columnar recombination on the alignment of the recoil momentum with the electric field can be experimentally demonstrated.

In this paper we study differential rates as a function of the nuclear recoil direction angle with respect to the vertical with no head-tail discrimination for a detector located at the Laboratori Nazionali del Gran Sasso and diurnal and seasonal modulations of such a signal.

With a likelihood-ratio based statistical approach we show that, using the angular information alone, 100 (250) events are sufficient to reject the isotropic hypothesis at 3 sigma level for a perfect (400 mrad) angular resolution. For an exposure of 100 tonne years, such as the detector described in [17], this number of events corresponds to a WIMP-nucleon cross section of about 10^{-46} cm^2 at 200 GeV WIMP mass. Larger exposures would probe directionality at smaller cross sections.

In view of the evidence presented in this paper, and in consideration of the strong exclusion bounds already achieved by null observations performed by non-directional dark matter detectors, it is of utmost importance the development of experimental technologies able to couple directional sensitivity with large fiducial masses (many tonnes) and the ability to collect large exposures free of background from β/γ events and neutron-induced nuclear recoils. One possible avenue would be offered by the presence of the signature of columnar recombination in nuclear recoils in a liquid argon time projection chamber, where this effect has already been observed for α particles and protons. Dedicated experiments performed on monochromatic, pulsed neutron beams will allow to explore the possible presence of this signature.

References

- [1] PLANCK collaboration, *Planck 2015 results. XIII. Cosmological parameters*, *Astron. Astrophys.* **594** (2016) A13 [[arXiv:1502.01589](#)] [[INSPIRE](#)].
- [2] V.C. Rubin, A.H. Waterman and J.D.P. Kenney, *Kinematic Disturbances in Optical Rotation Curves among 89 Virgo Disk Galaxies*, *Astron. J.* **118** (1999) 236.
- [3] D. Clowe et al., *A direct empirical proof of the existence of dark matter*, *Astrophys. J.* **648** (2006) L109 [[astro-ph/0608407](#)] [[INSPIRE](#)].
- [4] G. Covone et al., *Gauging the dark matter fraction in a L_* S0 galaxy at $z = 0.47$ through gravitational lensing from deep HST/ACS imaging*, *Astrophys. J.* **691** (2009) 531 [[arXiv:0809.4125](#)] [[INSPIRE](#)].
- [5] R.A. Malaney and G.J. Mathews, *Probing the early universe: A review of primordial nucleosynthesis beyond the standard Big Bang*, *Phys. Rept.* **229** (1993) 145 [[INSPIRE](#)].
- [6] F. Nesti and P. Salucci, *The Dark Matter halo of the Milky Way*, *AD 2013*, *JCAP* **07** (2013) 016 [[arXiv:1304.5127](#)] [[INSPIRE](#)].
- [7] C.T. Byrnes, M. Gerstenlauer, S. Nurmi, G. Tasinato and D. Wands, *Scale-dependent non-Gaussianity probes inflationary physics*, *JCAP* **10** (2010) 004 [[arXiv:1007.4277](#)] [[INSPIRE](#)].

- [8] J.D. Sloane, M.R. Buckley, A.M. Brooks and F. Governato, *Assessing Astrophysical Uncertainties in Direct Detection with Galaxy Simulations*, *Astrophys. J.* **831** (2016) 93 [[arXiv:1601.05402](#)] [[INSPIRE](#)].
- [9] J. Herzog-Arbeitman, M. Lisanti, P. Madau and L. Necib, *Empirical Determination of Dark Matter Velocities using Metal-Poor Stars*, *Phys. Rev. Lett.* **120** (2018) 041102 [[arXiv:1704.04499](#)] [[INSPIRE](#)].
- [10] L. Necib, M. Lisanti and V. Belokurov, *Dark Matter in Disequilibrium: The Local Velocity Distribution from SDSS-Gaia*, [arXiv:1807.02519](#) [[INSPIRE](#)].
- [11] G. Bertone, D. Hooper and J. Silk, *Particle dark matter: Evidence, candidates and constraints*, *Phys. Rept.* **405** (2005) 279 [[hep-ph/0404175](#)] [[INSPIRE](#)].
- [12] A.K. Drukier, K. Freese and D.N. Spergel, *Detecting Cold Dark Matter Candidates*, *Phys. Rev. D* **33** (1986) 3495 [[INSPIRE](#)].
- [13] K. Freese, J.A. Frieman and A. Gould, *Signal Modulation in Cold Dark Matter Detection*, *Phys. Rev. D* **37** (1988) 3388 [[INSPIRE](#)].
- [14] DAMA collaboration, *First results from DAMA/LIBRA and the combined results with DAMA/NaI*, *Eur. Phys. J. C* **56** (2008) 333 [[arXiv:0804.2741](#)] [[INSPIRE](#)].
- [15] R. Bernabei et al., *First Model Independent Results from DAMA/LIBRA-Phase2*, *Universe* **4** (2018) 116 [[arXiv:1805.10486](#)] [[INSPIRE](#)].
- [16] A. Tiwari, C. Zhang, D.M. Mei and P. Cushman, *Observation of annual modulation induced by γ rays from (α, γ) reactions at the Soudan Underground Laboratory*, *Phys. Rev. C* **96** (2017) 044609 [Erratum *ibid.* **C 98** (2018) 019901] [[arXiv:1706.00100](#)] [[INSPIRE](#)].
- [17] C.E. Aalseth et al., *DarkSide-20k: A 20 tonne two-phase LAr TPC for direct dark matter detection at LNGS*, *Eur. Phys. J. Plus* **133** (2018) 131 [[arXiv:1707.08145](#)] [[INSPIRE](#)].
- [18] F. Mayet et al., *A review of the discovery reach of directional Dark Matter detection*, *Phys. Rept.* **627** (2016) 1 [[arXiv:1602.03781](#)] [[INSPIRE](#)].
- [19] J.B.R. Battat et al., *Readout technologies for directional WIMP Dark Matter detection*, *Phys. Rept.* **662** (2016) 1 [[arXiv:1610.02396](#)] [[INSPIRE](#)].
- [20] XENON collaboration, *Dark Matter Search Results from a One Ton-Year Exposure of XENON1T*, *Phys. Rev. Lett.* **121** (2018) 111302 [[arXiv:1805.12562](#)] [[INSPIRE](#)].
- [21] D.R. Nygren, *Columnar recombination: a tool for nuclear recoil directional sensitivity in a xenon-based direct detection WIMP search*, *J. Phys. Conf. Ser.* **460** (2013) 012006 [[INSPIRE](#)].
- [22] G. Jaffé, *Zur Theorie der Ionisation in Kolonnen. II*, *Annalen Phys.* **393** (1929) 977.
- [23] V. Cataudella et al., *Directional modulation of electron-ion pairs recombination in liquid argon*, *2017 JINST* **12** P12002 [[INSPIRE](#)].
- [24] D.W. Swan, *Ionization of liquid argon by particles*, *Proc. Phys. Soc.* **85** (1965) 1297.
- [25] WARP collaboration, *Effects of Nitrogen contamination in liquid Argon*, *2010 JINST* **5** P06003 [[arXiv:0804.1217](#)] [[INSPIRE](#)].
- [26] SCENE collaboration, *Observation of the dependence on drift field of scintillation from nuclear recoils in liquid argon*, *Phys. Rev. D* **88** (2013) 092006 [[arXiv:1306.5675](#)] [[INSPIRE](#)].
- [27] SCENE collaboration, *Measurement of Scintillation and Ionization Yield and Scintillation Pulse Shape from Nuclear Recoils in Liquid Argon*, *Phys. Rev. D* **91** (2015) 092007 [[arXiv:1406.4825](#)] [[INSPIRE](#)].
- [28] J. Billard, F. Mayet and D. Santos, *Exclusion, Discovery and Identification of Dark Matter with Directional Detection*, *EAS Publ. Ser.* **53** (2012) 67 [[INSPIRE](#)].

- [29] S. Tassev and M. Zaldarriaga, *Estimating CDM Particle Trajectories in the Mildly Non-Linear Regime of Structure Formation. Implications for the Density Field in Real and Redshift Space*, *JCAP* **12** (2012) 011 [[arXiv:1203.5785](#)] [[INSPIRE](#)].
- [30] C.J. Copi and L.M. Krauss, *Angular signatures for galactic halo WIMP scattering in direct detectors: Prospects and challenges*, *Phys. Rev. D* **63** (2001) 043507 [[astro-ph/0009467](#)] [[INSPIRE](#)].
- [31] M. Cadeddu, *A directional Dark Matter argon detector at LNGS*, *J. Phys. Conf. Ser.* **689** (2016) 012015 [[INSPIRE](#)].
- [32] M. Cadeddu, *Dark Matter search with directional sensitivity*, *Nuovo Cim. C* **40** (2017) 66 [[INSPIRE](#)].
- [33] G. Fiorillo and M. Cadeddu, *Directionality in Dark Matter search*, *PoS(NOW2016)091* (2017).
- [34] R.H. Helm, *Inelastic and Elastic Scattering of 187-Mev Electrons from Selected Even-Even Nuclei*, *Phys. Rev.* **104** (1956) 1466 [[INSPIRE](#)].
- [35] P. Gondolo, *Recoil momentum spectrum in directional dark matter detectors*, *Phys. Rev. D* **66** (2002) 103513 [[hep-ph/0209110](#)] [[INSPIRE](#)].
- [36] M. Lisanti, L.E. Strigari, J.G. Wacker and R.H. Wechsler, *The Dark Matter at the End of the Galaxy*, *Phys. Rev. D* **83** (2011) 023519 [[arXiv:1010.4300](#)] [[INSPIRE](#)].
- [37] A. Blaauw, C.S. Gum, J.L. Pawsey and G. Westerhout, *The New I.A.U. System of Galactic Coordinates (1958 Revision)*, *Mon. Not. Roy. Astron. Soc.* **121** (1960) 123.
- [38] M.S. Alenazi and P. Gondolo, *Directional recoil rates for WIMP direct detection*, *Phys. Rev. D* **77** (2008) 043532 [[arXiv:0712.0053](#)] [[INSPIRE](#)].
- [39] LUX collaboration, *Results from a search for dark matter in the complete LUX exposure*, *Phys. Rev. Lett.* **118** (2017) 021303 [[arXiv:1608.07648](#)] [[INSPIRE](#)].
- [40] XENON collaboration, *First Dark Matter Search Results from the XENON1T Experiment*, *Phys. Rev. Lett.* **119** (2017) 181301 [[arXiv:1705.06655](#)] [[INSPIRE](#)].
- [41] PANDAX-II collaboration, *Dark Matter Results From 54-Ton-Day Exposure of PandaX-II Experiment*, *Phys. Rev. Lett.* **119** (2017) 181302 [[arXiv:1708.06917](#)] [[INSPIRE](#)].
- [42] M.J. Lewis and K. Freese, *The phase of the annual modulation: Constraining the WIMP mass*, *Phys. Rev. D* **70** (2004) 043501 [[astro-ph/0307190](#)] [[INSPIRE](#)].
- [43] K. Freese, M. Lisanti and C. Savage, *Colloquium: Annual modulation of dark matter*, *Rev. Mod. Phys.* **85** (2013) 1561 [[arXiv:1209.3339](#)] [[INSPIRE](#)].
- [44] J. Tatarowicz and C.J. Martoff, *Optimized running conditions and sensitivity for direction sensitive detectors of WIMP dark matter*, *Astropart. Phys.* **35** (2011) 235 [[INSPIRE](#)].
- [45] G. Cowan, K. Cranmer, E. Gross and O. Vitells, *Asymptotic formulae for likelihood-based tests of new physics*, *Eur. Phys. J. C* **71** (2011) 1.